Overlimiting Current in a Microchannel

E. Victoria Dydek,[1] Boris Zaltzman,[1,2] Isaak Rubinstein,[2] D. S. Deng,[1] Ali Mani,[1] and Martin Z. Bazant[1,3]

[1]*Department of Chemical Engineering, Massachusetts Institute of Technology, Cambridge, Massachusetts 02139, USA*
[2]*Blaustein Institutes for Desert Research, Ben-Gurion University of the Negev, Sede Boqer Campus, 84990, Israel*
[3]*Department of Mathematics, Massachusetts Institute of Technology, Cambridge, Massachusetts 02139, USA*

(Received 7 February 2011; published 6 September 2011)

We revisit the classical problem of diffusion-limited ion transport to a membrane (or electrode) by considering the effects of charged sidewalls. Using simple mathematical models and numerical simulations, we identify three basic mechanisms for overlimiting current in a microchannel: (i) surface conduction carried by excess counterions, which dominates for very thin channels, (ii) convection by electro-osmotic flow on the sidewalls, which dominates for thicker channels, and (iii) transitions to electro-osmotic instability on the membrane end in very thick channels. These intriguing electrokinetic phenomena may find applications in biological separations, water desalination, and electrochemical energy storage.

DOI: 10.1103/PhysRevLett.107.118301 PACS numbers: 47.57.jd, 47.20.Ma, 82.45.Gj

Introduction.—All electrochemical cells involve ion-selective surfaces, such as electrodes or membranes, that pass current carried by certain active ionic species [1]. In an unsupported bulk electrolyte, the rejection of the opposite species (to maintain neutrality) leads to salt depletion and ''concentration polarization'' (CP). Theoretically, at the diffusion-limited current, the solution conductivity vanishes at the surface, but in practice, ''overlimiting current'' (OLC) is often observed and associated with an extended depletion zone [Fig. 1(a)].

Possible mechanisms for OLC have been debated for decades. In the context of water electrodialysis [2], it is now understood that OLC can be due to chemical effects (water splitting or exaltation), which create additional ions, or a physical effect, electro-osmotic instability (EOI) [3], which enhances ion transport by convection [4] [Fig. 1(d)]. The flow is driven by extended space charge (ESC) in the nonequilibrium double layer on the selective surface [5]. Similar phenomena can also occur in dendritic electrodeposition [6], electrochromatography [7], and capacitive desalination at large voltages [8].

Some experiments have shown that CP is also affected by geometrical confinement. In thin-gap (100 μm) electrodeposition cells, gravitational and electro-osmotic convection can affect the spreading depletion layer [6]. In thinner microfluidic devices, steady depletion layers in transverse flows can form surprisingly sharp interfaces (''demixing''), whether triggered by capacitive desalination [9] or electrodialysis [10]. Additionally, convection can be suppressed by decreasing the channel height, thereby reducing (but not eliminating) OLC [11,12]. In very thin (1 μm) channels, it was recently shown that CP interfaces can propagate at constant current, analogous to shock waves in gases [13]. These ''desalination shocks'' result from geometry-dependent surface conduction [Fig. 1(b)] [14], but the role of convection and the connection with OLC have not been considered.

In this Letter, we develop a unified theory of steady CP in a microchannel (neglecting chemical effects) and identify physical mechanisms for OLC related to charged sidewalls. We show that surface conduction (SC) dominates in very narrow channels [Fig. 1(b)], while electro-osmotic flow (EOF) on the sidewalls dominates in wider channels [Fig. 1(c)] and transitions to EOI on the selective surface in very wide channels [Fig. 1(d)]. We are not aware of any

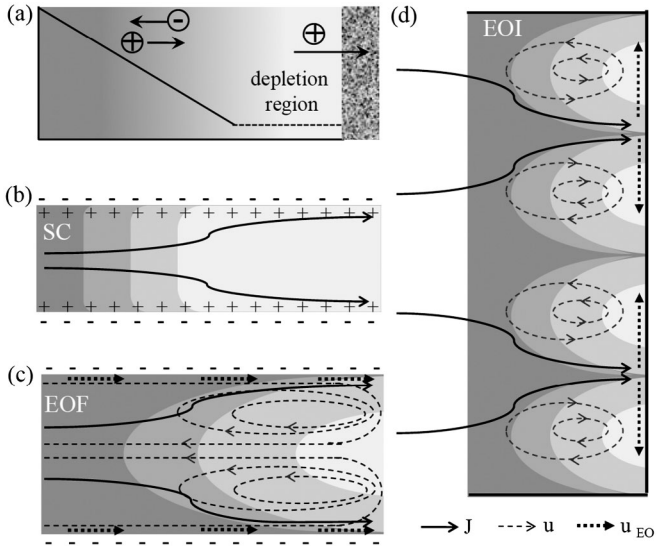

FIG. 1. Physical picture of overlimiting current (OLC) in a microchannel from a reservoir (left) to a cation-exchange membrane (right). The volume-averaged conductivity profile (a) exhibits a classical linear diffusion layer (continuous line) and a constant depleted region (dashed line), where the current is carried primarily by (b) SC, (c) EOF, or (d) EOI with increasing channel thickness.

prior mention of the SC mechanism for OLC, whereas our theory of the EOF mechanism differs from the recently proposed 1D Taylor-Aris dispersion model (strictly valid for aspect ratios $>10^3$ and zeta potentials >1 V) [15], by taking into account the 2D velocity field at the channel end.

Our analysis is based on the following model problem. A symmetric, binary z:z electrolyte fills a parallel-plate (2D) microchannel of length L and thickness H, which is open to a well-mixed reservoir of concentration c_0 at $x = 0$. A voltage V is applied across the microchannel to drive a current I through an ideal cation-selective solid surface (the "membrane") at $x = L$, which could represent a cation-exchange membrane, a negatively charged nanochannel, or a metal electrode undergoing electroplating. The sidewalls have a charge density $\sigma_s < 0$, which we take to be negative, as in most materials used in microfabrication (glass, silicones, silica, etc.). We shall see that the surface promotes OLC only if its charge has the same sign as the inactive species (anions).

Surface conduction.—As the channel thickness is decreased, convection eventually becomes negligible compared to diffusion (small Péclet number), so we begin by considering only "surface conduction" associated with the excess counterions (active cations) that screen the wall charge [15,16], neglecting streaming current (which we analyzed separately [17]). For long, narrow channels ($H \ll L$), and thin double layers ($\lambda_D \ll H$, where λ_D is the Debye screening length), the Nernst-Planck equations can be homogenized (area averaged) as follows [14,18,19]:

$$\frac{dc_+}{dx} + c_+ \frac{d\tilde{\phi}}{dx} = -\frac{j}{zeD}, \qquad \frac{dc_-}{dx} - c_- \frac{d\tilde{\phi}}{dx} = 0, \quad (1)$$

$$c = c_- = c_+ + \frac{\rho_s}{e}, \quad (2)$$

where c_+ and c_- are the mean concentrations of cations and anions, respectively, D is the ionic diffusivity (for simplicity, the same for both species), $\tilde{\phi}$ is dimensionless potential scaled to the thermal voltage, kT/ze. Equation (1) relates the cation flux to the current density j in steady state for a perfect cation-selective surface. Equation (2) is a mean electroneutrality condition including both ionic and fixed surface charges, where $\rho_s = 2\sigma_s/H$ is the negative volume density of fixed charge.

The homogenized 1D model can be solved analytically:

$$\tilde{\phi} = \ln(\tilde{c}), \qquad \tilde{c} - \tilde{\rho}_s \ln(\tilde{c}) = 1 - \tilde{j}x, \quad (3)$$

$$\tilde{j} = 1 - e^{-\tilde{V}} - \tilde{\rho}_s \tilde{V}, \quad \text{(SC)} \quad (4)$$

where $\tilde{\rho}_s = \frac{\rho_s}{2zec_0}$ is dimensionless fixed-charge density, $\tilde{j} = \frac{jL}{2zeDc_0}$ is the dimensionless current density scaled by the limiting current, corresponding to the case with neutral sidewalls; $\tilde{c} = c/c_0$, $\tilde{x} = x/L$, and voltage $\tilde{V} = zeV/kT = -\tilde{\phi}(1)$ is the potential drop across the electrolyte, relative to $\tilde{\phi}(0) = 0$ at the reservoir. The current-voltage relationship, Eq. (4), is shown in Fig. 2(a) demonstrating nearly constant conductance in the OLC regime. For small surface charge and/or wide channels, $0 < -\tilde{\rho}_s \ll 1$, the anion concentration profile (3) is linear in the quasineutral bulk region, $\tilde{c} \sim 1 - \tilde{j}x$, and decays exponentially, $\tilde{c} \sim e^{(\tilde{j}x-1)/\tilde{\rho}_s}$, in the depleted zone, $\tilde{j}^{-1} < x < 1$, that forms above the limiting current, as shown in Fig. 2(b). In the opposite "membrane limit," $-\tilde{\rho}_s \gg 1$, the concentration is only weakly perturbed by the current, $\tilde{c} \sim 1 + (\tilde{j}x - 1)/\tilde{\rho}_s$.

As shown in Fig. 2(c), the current-voltage relation (4) can be interpreted as an ideal diode, $\tilde{j}_b = 1 - e^{-\tilde{V}}$, for bulk CP in parallel with a shunt resistance, $\tilde{j}_s = -\tilde{\rho}_s \tilde{V}$, for SC. The electric field, which is nearly uniform across the microchannel, acts on two different types of ions: (i) the inert anions plus an equal number of cations ("bulk conductivity"), and (ii) the remaining cations that screen the surface charge ("surface conductivity"). The response is equivalent to that of an ideal Schottky diode (metal-superconductor junction) [20] with the surface charge playing the role of a n-type dopant in the semiconductor, which provides a residual conductivity under reverse bias. As the microchannel thickness is increased, convection due to EOF eventually dominates SC, and the semiconductor analogy breaks down.

Electro-osmotic flow.—For our "dead-end channel" with an impermeable membrane, pressure-driven back flow opposes EOF and results in two counterrotating vortices. Concentrated solution flows to the membrane along the sidewalls, and depleted solution returns in the center [Fig. 1(c)].

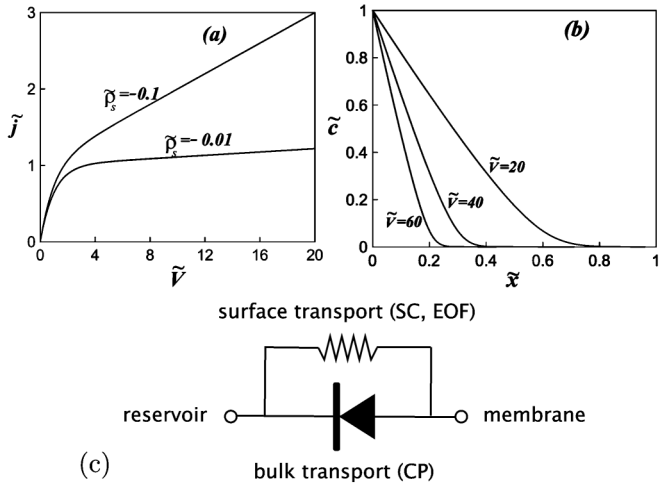

FIG. 2. Overlimiting current in the surface conduction regime: (a) Dimensionless current-voltage relation, Eq. (4), for $\tilde{\rho}_s = -0.01, -0.1$ and (b) mean concentration profile of inert anions, Eq. (3), for $\tilde{\rho}_s = -0.1$. (c) The equivalent circuit: an ideal diode for bulk CP in parallel with a constant shunt resistance for SC (or EOF, as in Fig. 3).

As a first approximation, we assume thin double layers and a neutral bulk solution ($c = c_- = c_+$) described by the steady 2D Nernst-Planck-Stokes equations,

$$\mathbf{u} \cdot \boldsymbol{\nabla} c = -\boldsymbol{\nabla} \cdot \mathbf{F}_{\pm}, \qquad \mathbf{F}_{\pm} = -D(\boldsymbol{\nabla} c \pm c \boldsymbol{\nabla} \tilde{\phi}) \quad (5)$$

$$\boldsymbol{\nabla} p = \eta \boldsymbol{\nabla}^2 \mathbf{u}, \qquad \boldsymbol{\nabla} \cdot \mathbf{u} = 0 \quad (6)$$

where $\mathbf{u}$ is the fluid velocity, η the viscosity, and p the pressure with boundary conditions of no slip, $\mathbf{u} = \mathbf{0}$, and vanishing normal coion flux and specify uniform electrochemical potential of counterions at the membrane corresponding to potentiostatic operating conditions; uniform concentration $c(0, y) = c_0$ and zero pressure at the reservoir; and zero normal flux (neglecting SC) and EOF slip at $y = \pm H/2$ given by the Helmholtz-Smoluchowski formula (neglecting diffusio-osmosis [4]),

$$\mathbf{u}_x = \frac{\varepsilon \zeta}{\eta} \frac{\partial \phi}{\partial x}, \qquad \zeta = \frac{\sigma_s \lambda_D}{\varepsilon}, \qquad \lambda_D(c) = \sqrt{\frac{\varepsilon k_B T}{2(ze)^2 c}}, \quad (7)$$

where $\zeta(c)$ is the zeta potential in the Debye-Hückel approximation and ε, the permittivity. The main output parameter in model (5)–(7), the dimensionless current $\tilde{j}$ depends on the dimensionless channel thickness, $\tilde{H} = \frac{H}{L}$, reservoir Debye length, $\tilde{\lambda}_0 = \frac{\lambda_D(c_0)}{L}$, surface charge, $\tilde{\sigma}_s = \tilde{\rho}_s \tilde{H}$, and voltage, $\tilde{V} = \frac{zeV}{kT}$.

Numerical solutions [17] of (5)–(7) are shown in Fig. 3. An interesting observation about CP during OLC follows from averaging the 2D concentration profile [Fig. 3(a)] over the channel cross section [Fig. 3(b)]. The intense vortical circulation near the dead end forms an extended depletion zone with a nearly constant area-averaged concentration, $c_d = \tilde{c}_d c_0$, as the case of electro-osmotic instability (EOI) without geometrical confinement [3]. For moderate aspect ratios, $\tilde{H}^{-1} < 10$, the dimensionless distance of the vortex center from the membrane, $\tilde{l}_c = l/L$, is nearly independent of voltage in the OLC regime [inset of Fig. 3(b)] and approximately equal to the dimensionless concentration $\tilde{c}_d \approx \tilde{l}_c$.

Using this observation, we can derive a 1D model for the EOF regime [17] [inset of Fig. 3(c)] which yields an approximate OLC current-voltage relation,

$$\tilde{j} \approx 1 - \tilde{c}_d^2 + 2\tilde{c}_d \ln \tilde{c}_d + \tilde{c}_d \tilde{V} \quad \text{(EOF)} \quad (8)$$

which compares well with our 2D simulations [Fig. 3(c)] for $\tilde{H} > 0.1$ [17]. The linear dependence of (8) again implies a constant shunt resistance [Fig. 2(c)] for the EOF mechanism, $\tilde{j}_s = \tilde{c}_d \tilde{V}$, as in (4) for the SC mechanism, but with a different overlimiting conductance, $\tilde{c}_d$ rather than $-\tilde{\rho}_s$.

To understand the overlimiting conductance, we perform a scaling analysis of the 2D model [17]. Balancing axial convection over the length scale l_c with transverse diffusion over the scale H in (5), the vortex position scales as $l_c \sim u_{\mathrm{EOF}} H^2/D$. The characteristic EOF velocity along the walls scales as $u_{\mathrm{EOF}} \sim \tilde{\sigma}_s \tilde{j} u_{\mathrm{ref}}/\tilde{c}^{3/2} \tilde{\lambda}_0$, where we use (7) and define the reference (electroviscous) velocity scale, $u_{\mathrm{ref}} = \varepsilon (kT/e)^2/\eta L$. The numerical observation $\tilde{c}_d \approx \tilde{l}_c$ then implies the following scaling relation near limiting current ($\tilde{j} \approx 1$):

$$\tilde{c}_d \approx \tilde{l}_c \approx 0.22 \tilde{\sigma}_s^{2/5} \tilde{H}^{4/5} \tilde{\lambda}_0^{-2/5}, \quad (9)$$

which shows how the overlimiting conductance due to EOF varies with surface charge, channel thickness, and reservoir concentration (via λ_0). Our 2D simulations (Fig. 4, inset) roughly confirm the scaling of $\tilde{c}_d \approx \tilde{l}_c$

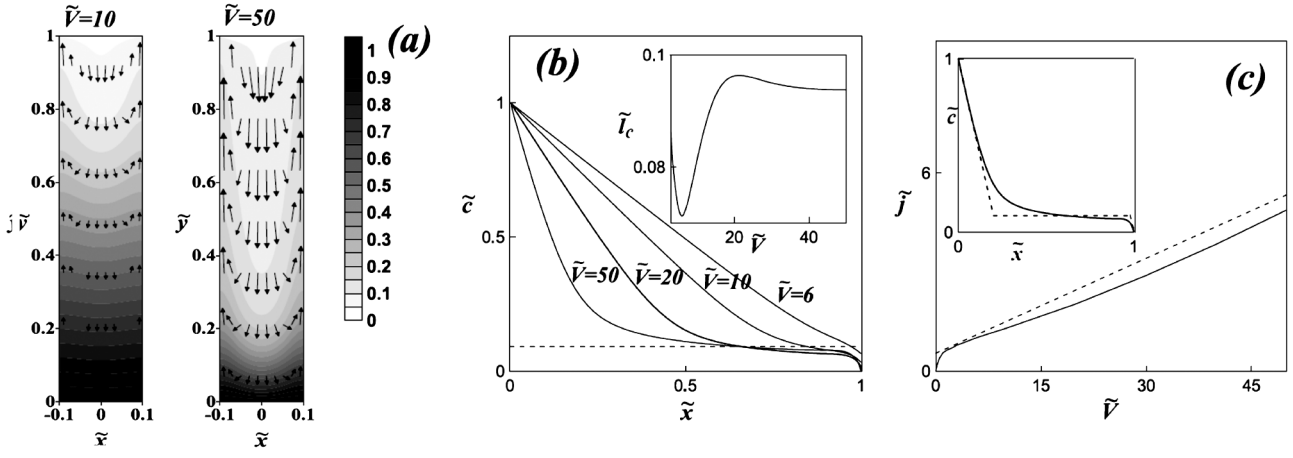

FIG. 3. 2D simulations of the EOF mechanism for OLC ($\tilde{\lambda}_0 = 0.01$, $\tilde{H} = 0.2$, $\tilde{\sigma}_s = -0.01$): (a) bulk salt concentration $\tilde{c}$ (contours) and velocity vectors $\mathbf{u}$ (arrows); (b) area-averaged concentration profiles (continuous), showing a nearly constant depleted-zone concentration $\tilde{c}_d \approx \tilde{l}_c$. Inset: vortex position $\tilde{l}_c$ vs voltage $\tilde{V}$; (c) current-voltage relation from simulations (continuous) and the 1D model (8) (dashed). Inset: area-averaged concentration profile in the 2D simulations (continuous) and in 1D model (dashed) for $\tilde{V} = 50$.

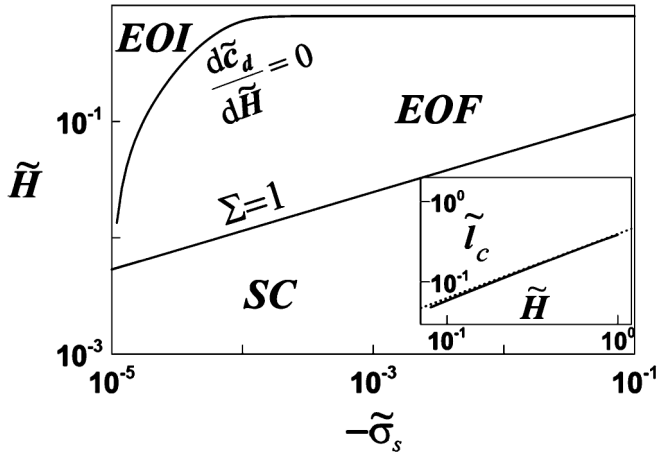

FIG. 4. The regions of dominance of the SC, EOF, and EOI mechanisms for varying channel aspect ratio, $\tilde{H}^{-1}$ and surface charge $\tilde{\sigma}_s$ for $\tilde{\lambda}_0 = 10^{-5}$. The critical value of $\tilde{H}$ is given by $\Sigma = 1$ in (10) for the SC/EOF transition and by $\frac{d\tilde{c}_d}{d\tilde{H}} = 0$ in 2D simulations for the EOF/EOI transition. Inset: Simulated vortex center location $\tilde{l}_c$ versus $\tilde{H}$ for $\tilde{\lambda}_0 = 0.01$, $\tilde{\sigma}_s = -0.1$ (solid) compared to the scaling law, $\tilde{l}_c = 0.38\tilde{H}^{4/5}$ in (9).

with $\tilde{H}$ and provide the prefactor in (9). For very large currents ($\tilde{j} \gg 1$), the conductance is predicted to increase [17] [Fig. 3(c)], but a detailed analysis also considering high aspect ratios ($\tilde{H}^{-1} \gg 10$) is left for future work.

Unified scaling analysis.—The relative importance of the SC and EOF mechanisms for OLC is controlled by the dimensionless ratio of their conductances in the weakly overlimiting regime, $\Sigma = |\tilde{\rho}_s|/\tilde{c}_d$. Using (9) and restoring dimensional variables, we obtain the scaling

$$\Sigma \approx 8\tilde{\lambda}_0^{2/5}|\tilde{\sigma}_s|^{3/5}\tilde{H}^{-9/5} \sim H^{-9/5}L^{4/5}|\sigma_s^{3/5}|c_0^{-4/5}, \quad (10)$$

where $\Sigma = 1$ marks the transition between mechanisms (Fig. 4). Equation (10) shows that SC dominates for thin channels, low ion concentration, and/or large surface charge ($\Sigma \gg 1$), while EOF dominates above a critical channel thickness and/or salt concentration ($\Sigma \ll 1$).

As the channel thickness is increased further, surface effects eventually become negligible, and OLC results from bulk EOI at the membrane, as in unconfined systems [3,4]. The EOF vortex intensity, scaling as $\tilde{l}_c/\tilde{H} \sim H^{-1/5}$ from (9), decreases with $\tilde{H}$, and thus, above a critical channel thickness, a significant portion of the depleted solution near the membrane is unaffected by EOF and instead undergoes EOI to maintain OLC. EOI also leads to a constant overlimiting conductance (beyond a threshold voltage) [3,4], so the EOF/EOI transition can be defined via $\frac{d\tilde{c}_d}{d\tilde{H}} = 0$ in our 2D simulations, above which the EOF supply of solute to the membrane fades and conditions develop for EOI (Fig. 4 and Supplementary Material, Fig. S4 [17]). In water, for $L = 1$ mm, $\zeta_0 = 50$ mV, and $c_0 = 1$ mM, the predicted mechanism for OLC transitions from SC to EOF at $H = 8$ μm (consistent with observed vortex suppression [11]) and from EOF to EOI at $H = 0.4$ mm, so that different microfluidic experiments can be dominated by SC [13], EOF [10], or EOI [3].

Conclusion.—In a microchannel, charged sidewalls can sustain OLC to an ion-selective end. With increasing channel thickness, the dominant mechanism switches from SC to EOF to EOI. These nonlinear phenomena may find applications in water desalination, biological separations, or electrochemical energy storage.

This work was supported by a seed grant from the MIT Energy Initiative and by the Israel Science Foundation (Grant No. 65/07).

[1] R. F. Probstein, *Physicochemical Hydrodynamics* (Wiley, New York, 2003); J. Newman and K. E. Thomas-Alyea, *Electrochemical Systems* (Wiley, New York, 2004).
[2] V. V. Nikonenko *et al.*, Adv. Colloid Interface Sci. **160**, 101 (2010).
[3] I. Rubinstein and B. Zaltzman, Phys. Rev. E **62**, 2238 (2000); B. Zaltzman and I. Rubinstein, J. Fluid Mech. **579**, 173 (2007); S. M. Rubinstein *et al.*, Phys. Rev. Lett. **101**, 236101 (2008).
[4] S. S. Dukhin, N. A. Mishchuk, and P. B. Takhistov, Colloid J. USSR **51**, 616 (1989); I. Rubinshtein *et al.*, Russ. J. Electrochem. **38**, 853 (2002); G. Yossifon and H. C. Chang, Phys. Rev. Lett. **101**, 254501 (2008).
[5] W. H. Smyrl and J. Newman, Trans. Faraday Soc. **63**, 207 (1967); I. Rubinstein and L. Shtilman, J. Chem. Soc. Faraday Trans. II **75**, 231 (1979); K. T. Chu and M. Z. Bazant, SIAM J. Appl. Math. **65**, 1485 (2005).
[6] J. M. Huth *et al.*, Phys. Rev. E **51**, 3444 (1995); M. Rosso, Electrochim. Acta **53**, 250 (2007).
[7] U. Tallarek, F. C. Leinweber, and I. Nischang, Electrophoresis **26**, 391 (2005).
[8] M. Z. Bazant, K. Thornton, and A. Ajdari, Phys. Rev. E **70**, 021506 (2004); L. H. Olesen, M. Z. Bazant, and H. Bruus, Phys. Rev. E **82**, 011501 (2010); P. M. Biesheuvel and M. Z. Bazant, Phys. Rev. E **81**, 031502 (2010).
[9] F. Leinweber *et al.*, Anal. Chem. **78**, 1425 (2006).
[10] Y. C. Wang, A. Stevens, and J. Han, Anal. Chem. **77**, 4293 (2005); S. J. Kim *et al.*, Nature Nanotech. **5**, 297 (2010).
[11] S. J. Kim *et al.*, Phys. Rev. Lett. **99**, 044501 (2007).
[12] G. Yossifon, P. Mushenheim, and H. C. Chang, Europhys. Lett. **90**, 64004 (2010).
[13] A. Mani, T. A. Zangle, and J. G. Santiago, Langmuir **25**, 3898 (2009); T. A. Zangle, A. Mani, and J. G. Santiago, Langmuir **25**, 3909 (2009).
[14] A. Mani and M. Z. Bazant, arXiv:1108.0871v1.
[15] A. Yaroshchuk, E. Zholkovskiy, S. Pogodin, and V. Baulin, Langmuir (in press).
[16] B. V. Deryagin and S. S. Dukhin, Kolloid Z. **31**, 350 (1969) [Colloid J. USSR **31**, 277 (1969)]; J. J. Bikerman, Kolloid Z. **72**, 100 (1935); K. T. Chu and M. Z. Bazant, J. Colloid Interface Sci. **315**, 319 (2007).

[17] See Supplemental Material at http://link.aps.org/supplemental/10.1103/PhysRevLett.107.118301 for scaling analysis and simulation details.

[18] F. Helfferich, *Ion Exchange* (McGraw-Hill, New York, 1962); F. Helfferich, *Ion Exchange* reprinted by (Dover, New York, 1995).

[19] P. Ramírez *et al.*, J. Chem. Phys. **126**, 194703 (2007); N. R. Scruggs *et al.*, Nano Lett. **9**, 3853 (2009); A. Szymczyk, H. Zhu, and B. Balannec, Langmuir **26**, 1214 (2010).

[20] S. M. Sze and K. K. Ng, *Physics of Semiconductor Devices* (Wiley, New Jersey, 2007).